Hybrid RIS-Empowered Reflection and Decode-and-Forward Relaying for Coverage Extension

Ibrahim Yildirim, *Graduate Student Member, IEEE*, Fatih Kilinc, *Student Member, IEEE*, Ertugrul Basar, *Senior Member, IEEE*, and George C. Alexandropoulos, *Senior Member, IEEE*

***Abstract*— In this letter, we introduce two hybrid transmission schemes combining a passive reconfigurable intelligent surface (RIS) with decode-and-forward relaying in a synergistic manner. The proposed schemes offer a flexible as well as cost- and power-efficient solution for coverage extension in future generation wireless networks. We present closed-form expressions for the end-to-end signal-to-noise ratio of both schemes and a sequential optimization algorithm for the power allocation and the RIS phase configurations. Our computer simulations and theoretical analysis demonstrate that the RIS and relaying technologies enhance the achievable rate and error performance remarkably when working complementary to each other, rather than being considered as competing technologies.**

***Index Terms*— 6G, relaying, reconfigurable intelligent surface.**

I. Introduction

In order to fulfill the stringent requirements of the upcoming Internet-of-Everything (IoE) era, reconfigurable intelligent surfaces (RISs) have been regarded as one of the key technologies, owing to their capability to reconfigure the propagation environment with software-controlled reflection [1]–[3].

RIS-empowered wireless transmission has recently drawn substantial attention from both academia and industry [4]–[6]. There are many research efforts examining the differences between RIS and relaying technologies. Although RISs and relaying are similar technologies to enhance the system performance, the received signal is actively processed at the relay, while the RIS only reflects the incident signal without any active transmit module [7]. In [8], half-duplex (HD) decode-and-forward (DF) relaying and RIS-assisted transmission are compared in terms of energy efficiency, and it has been shown that the performance of a relay is achievable when hundreds of reflectors are used at the RIS. Moreover, a full-duplex (FD) relay-assisted system comprising two horn antennas and two RISs very close to the relay has been proposed in [9], and improvements in achievable rate are achieved even with a low number of reflective elements. However, the consideration of two horn antennas for the FD relay will cause high hardware cost, rendering end-to-end channel estimation difficult in the case of large numbers of transmission nodes and terminals. In [10], the authors proposed a hybrid transmission scenario combining a DF relay with an RIS and showed that using a single relay for low signal-to-noise ratio (SNR) values outperforms an RIS with massive number of reflectors, while for high SNRs, RIS-assisted transmissions are preferable. Recently in [11], RIS and FD relay are combined to provide reliable transmission and a semi-definite relaxation-based approach is proposed to cope with a non-convex optimization problem.

As pointed out in the previous discussion, most of the studies related to relaying and RISs consider the one of these technologies as an alternative solution to the other. Against this background, in this study, we aim to find the best transmission scenarios where these two exciting technologies work in harmony with each other. Our main motivation is to design hybrid RIS- and relay-aided systems with low operational complexity, while keeping the advantages of RIS and relaying technologies. To this end, two different cost efficient scheme are proposed for coverage extension by avoiding multi-hop relaying, and the best positioning for the RIS and the relay are investigated by considering that the direct communication link between the end terminals is blocked.

II. System and Channel Models

In this section, we introduce the proposed hybrid RIS and relay-assisted schemes as well as provide their working principles. Two novel hybrid transmission concepts are proposed by considering that an RIS and a DF relay are placed between the source (S) and the destination (D). It is assumed that the relay operates in HD mode, the RIS consists of N reflecting elements and the intelligent phase adjustment of the RIS is performed under perfect channel state information. Furthermore, all wireless channels are assumed to exhibit Rician fading with a factor of K.

A. Joint RIS and Relay Transmission Scheme

The system model of the joint RIS and relay transmission scheme is illustrated in Fig. 1. As seen from Fig. 1, S and D are equipped with a single antenna and the channels between the S-D link and the S-relay link are not available due to the blockage. Since the signals at the millimeter and THz frequencies are highly vulnerable to the blockage, the reliability of transmission at high distances can be compromised. In this scenario, the coverage area of the communication is extended

Manuscript received December 22, 2020; revised January 19, 2021; accepted January 24, 2021. Date of publication January 26, 2021; date of current version May 6, 2021. This work was supported by TUBITAK under Grant 120E401. The associate editor coordinating the review of this letter and approving it for publication was M. Wen. *(Corresponding author: Ertugrul Basar.)*

Ibrahim Yildirim is with the Faculty of Electrical and Electronics Engineering, Istanbul Technical University, 34469 Istanbul, Turkey, and also with the Department of Electrical and Electronics Engineering, Koç University, 34469 Istanbul, Turkey (e-mail: yildirimib@itu.edu.tr).

Fatih Kilinc and Ertugrul Basar are with the CoreLab, Department of Electrical and Electronics Engineering, Koç University, 34469 Istanbul, Turkey (e-mail: fkilinc20@ku.edu.tr; ebasar@ku.edu.tr).

George C. Alexandropoulos is with the Department of Informatics and Telecommunications, National and Kapodistrian University of Athens, 15784 Athens, Greece (e-mail: alexandg@di.uoa.gr).

Digital Object Identifier 10.1109/LCOMM.2021.3054819

Notation: Boldface lowercase and capital letters, respectively, represent vectors and matrices. The transpose of $\mathbf{A}$ is represented by $\mathbf{A}^T$ and $\mathbb{C}$ is the complex number set. $\mathbb{E}[.]$ and $|.|$ denote the expected and absolute values. $\mathcal{CN}(\mu, \sigma^2)$ denotes a complex Gaussian distributed random variable with μ mean and σ^2 variance.

1558-2558 © 2021 IEEE. Personal use is permitted, but republication/redistribution requires IEEE permission.
See https://www.ieee.org/publications/rights/index.html for more information.

Authorized licensed use limited to: ULAKBIM UASL - KOC UNIVERSITY. Downloaded on May 09,2021 at 19:32:20 UTC from IEEE Xplore. Restrictions apply.

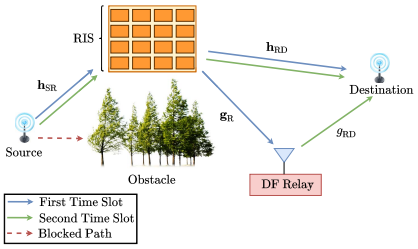

Fig. 1. The system model of the joint RIS and DF relay transmission scheme where the RIS and the relay are placed close to the S and D, respectively.

by placing an RIS in a position close to S, while it is aimed to reach the signal via the DF relay placed close to D.

In the first time-slot, the received signal at the relay and D are respectively given by

$$y_{\text{R}} = \sqrt{P_1}\mathbf{g}_{\text{R}}^T\mathbf{\Phi}_1\mathbf{h}_{\text{SR}}s + n_{\text{R}}, \tag{1}$$

$$y_{\text{D}}^I = \sqrt{P_1}\mathbf{h}_{\text{RD}}^T\mathbf{\Phi}_1\mathbf{h}_{\text{SR}}s + n_{\text{D}}^I \tag{2}$$

where $\mathbf{g}_{\text{R}} \in \mathbb{C}^{N\times 1}$, $\mathbf{h}_{\text{SR}} \in \mathbb{C}^{N\times 1}$, and $\mathbf{h}_{\text{RD}} \in \mathbb{C}^{N\times 1}$ are the fading channel coefficients between the RIS-relay, S-RIS, and RIS-D links, P_1 is the transmission power of S, $\mathbf{\Phi}_1 = \text{diag}\left\{e^{j\phi_1^1}, \ldots, e^{j\phi_1^N}\right\}$, with ϕ_1^i being the phase shift introduced by ith element of the RIS in the first time slot, s is the transmitted signal from S with unit-average-power ($\mathbb{E}[|s|^2] = 1$), n_{R} and n_{D}^I are the additive white Gaussian noise (AWGN) terms at the relay and D, which are distributed according to $\mathcal{CN}(0, N_0)$.

Assuming that the DF relay has a perfect decoding capability, the received signal at D in the second time slot can be expressed as follows:

$$y_{\text{D}}^{II} = \sqrt{P_2}\mathbf{h}_{\text{RD}}^T\mathbf{\Phi}_2\mathbf{h}_{\text{SR}}s + \sqrt{P_3}g_{\text{RD}}s + n_{\text{D}}^{II} \tag{3}$$

where $g_{\text{RD}} \in \mathbb{C}$ is the fading channel coefficient between the relay-D link, P_2 and P_3 are respectively the transmission power of S and the relay in the second time slot, $\mathbf{\Phi}_2 = \text{diag}\left\{e^{j\phi_2^1}, \ldots, e^{j\phi_2^N}\right\}$, with ϕ_2^i being the phase shift of ith element of the RIS in the second time slot and n_{D}^{II} is the AWGN term distributed according to $\mathcal{CN}(0, N_0)$. In (3), the first term is denotes the RIS-based signal, while the second term represents the signal transmitted by the relay after perfectly decoded as s.

By considering intelligent phase shifting capability of the RIS, the maximized received SNR at D in the first time slot is expressed by

$$\gamma_1 = \max_{\mathbf{\Phi}_1} \frac{P_1\left|\mathbf{h}_{\text{RD}}^T\mathbf{\Phi}_1\mathbf{h}_{\text{SR}}\right|^2}{N_0} = \frac{P_1\left|\sum_{i=1}^{N}|h_{\text{RD,i}}||h_{\text{SR,i}}|\right|^2}{N_0} = \frac{P_1A^2}{N_0} \tag{4}$$

where A has the Gaussian distribution for $N \gg 1$ due to central limit theorem (CLT) with the following mean and variance [6]:

$$\mu_A = \frac{N\sqrt{P_L^{R_1}}\pi}{4(K+1)}L_{1/2}^2(-K),$$

$$\sigma_A^2 = NP_L^{R_1} - \frac{NP_L^{R_1}\pi^2}{16(K+1)^2}L_{1/2}^4(-K) \tag{5}$$

where $P_L^{R_1}$ is the path loss for the S-D link and $L_n(x) = \frac{e^x}{n!}\frac{d^n}{dx^n}(e^{-x}x^n)$ is the Laguerre polynomials of degree n. Since γ_1 is a non-central chi-square distributed random variable with one degree of freedom, its moment generating function (MGF) is calculated by

$$M_{\gamma_1}(s) = \left(1 - \frac{sNP_L^{R_1}\left[16(K+1)^2 - \pi^2L_{1/2}^4(-K)\right]P_1}{8(K+1)^2N_0}\right)^{-1/2} \times \exp\left(\frac{\frac{sP_L^{R_1}N^2\pi^2L_{1/2}^4(-K)P_1}{16(K+1)^2N_0}}{1 - \frac{sNP_L^{R_1}\left[16(K+1)^2 - \pi^2L_{1/2}^4(-K)\right]P_1}{8(K+1)^2N_0}}\right). \tag{6}$$

By considering the similar phase adjustment in the first time slot and assuming $P_2 = P_3$ due to simplicity, the maximized received SNR at the D in the second time slot is obtained as

$$\gamma_2 = \max_{\mathbf{\Phi}_2} \frac{P_2\left|g_{RD} + \mathbf{h}_{\text{RD}}^T\mathbf{\Phi}_2\mathbf{h}_{\text{SR}}\right|^2}{N_0} = \frac{P_2\left||g_{RD}| + \sum_{i=1}^{N}|h_{\text{RD,i}}||h_{\text{SR,i}}|\right|^2}{N_0} = \frac{P_2B^2}{N_0}. \tag{7}$$

Here, due to the Lyapunov variant of the CLT [12], B is a Gaussian distributed random variable for $N \gg 1$ with the following mean and variance respectively

$$\mu_B = P_L^D\sqrt{\frac{\pi}{4(K+1)}}L_{1/2}(-K) + \frac{N\sqrt{P_L^{R_1}}\pi}{4(K+1)}L_{1/2}^2(-K),$$

$$\sigma_B^2 = P_L^D - \frac{P_L^D\pi L_{1/2}^2(-K)}{(K+1)} + NP_L^{R_1} - \frac{NP_L^{R_1}\pi^2L_{1/2}^4(-K)}{16(K+1)^2} \tag{8}$$

where P_L^D is the path loss for the relay-D link. Similar to γ_1, γ_2 follows the non-central chi-square distribution with one degree of freedom and its MGF is calculated by

$$M_{\gamma_2}(s) = \left(1 - \frac{2s\sigma_B^2P_2}{N_0}\right)^{-1/2}\exp\left(\frac{s\mu_B^2P_2/N_0}{1 - 2s\sigma_B^2P_2/N_0}\right). \tag{9}$$

B. Integrated RIS and Relay Transmission Scheme

In this hybrid scheme, we propose a transmission scheme where the RIS and the relay are integrated in the same device and positioned in between S and D as shown in Fig. 2. In contrast to the joint RIS and relaying scenario, we assume that S's signal reaches the RIS-relay device, which is both reflected and DF relayed to D. We again assume here that the distance between S and D is considerably large, hence, the S-D direct communication link is blocked.

In the first time-slot of the integrated RIS and relay transmission scheme, the received signal at the relay and D are respectively given by

$$y_{\text{R}} = \sqrt{P_1}g_{\text{SR}}s + n_{\text{R}}, \tag{10}$$

$$y_{\text{D}}^I = \sqrt{P_1}\mathbf{h}_{\text{RD}}^T\mathbf{\Phi}_1\mathbf{h}_{\text{SR}}s + n_{\text{D}}^I, \tag{11}$$

where $g_{\text{SR}} \in \mathbb{C}$, $\mathbf{h}_{\text{SR}} \in \mathbb{C}^{N\times 1}$ and $\mathbf{h}_{\text{RD}} \in \mathbb{C}^{N\times 1}$ are the fading channel coefficients between the S-relay, S-RIS and RIS-D links, P_1 is the transmission power of S, s is the transmitted signal from S with the unit-average-power, n_{R} and n_{D}^I are the

Authorized licensed use limited to: ULAKBIM UASL - KOC UNIVERSITY. Downloaded on May 09,2021 at 19:32:20 UTC from IEEE Xplore. Restrictions apply.

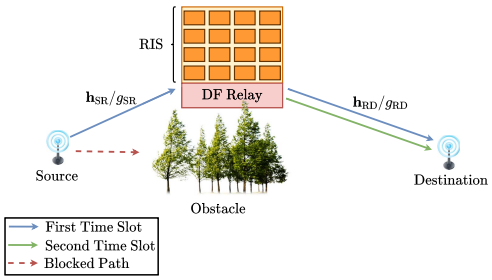

Fig. 2. The system model of the integrated RIS and DF relay transmission scheme.

AWGN at the relay and D, which are distributed according to $\mathcal{CN}(0, N_0)$.

The received signal transmitted through the perfect DF relay in the second time slot is obtained as

$$y_{\text{D}}^{II} = \sqrt{P_2} g_{\text{RD}} s + n_{\text{D}}^{II}, \tag{12}$$

where g_{RD} is the fading channel coefficients between the relay-D link, $P_2$is the transmission power of relay in the second time slot, and n_{D}^{II} is the AWGN as $n \sim \mathcal{CN}(0, N_0)$.

Similar to the joint RIS and relay case, the received SNR in the first time slot is expressed as in (4). Therefore, MGF of γ_1 is obtained as in (6) for integrated RIS and relay transmission. Furthermore, the received SNR at the D in the second time slot is given by $\gamma_2 = P_2 \left|g_{\text{RD}}\right|^2 / N_0$ where γ_2 has non-central chi-square distribution with two degrees of freedom and its MGF is expressed as

$$M_{\gamma_2}(s) = \left(1 - \frac{P_2 P_L^D}{2(K+1)N_0}\right)^{-1/2} \times \exp\left(\frac{2sP_2P_L^D K}{2(K+1)N_0 - P_2P_L^D}\right). \tag{13}$$

III. Performance Analysis and Sequential Optimization

In this section, theoretical average symbol error probability (SEP) and achievable rate expressions of the joint and integrated RIS and relay schemes are evaluated under the ideal DF relay assumption. Further, a sequential optimization algorithm is proposed to maximize the achievable rate of these hybrid schemes under non-ideal relay assumption. By considering the maximum likelihood detection rule, the received signals can be combined by using the maximal ratio combining (MRC) technique for both schemes, and the total SNR at D can be obtained as $\gamma_{\text{tot}} = \gamma_1 + \gamma_2$. Therefore, the MGF of the total SNR is calculated by $M_{\gamma_{\text{tot}}}(s) = M_{\gamma_1}(s) M_{\gamma_2}(s)$. Thus, the average (SEP) of the proposed schemes for M-phase shift keying (PSK) signaling (as a representative example) is obtained as [13]

$$P_e = \frac{1}{\pi} \int_0^{(M-1)\pi/M} M_{\gamma_{\text{tot}}}\left(-\frac{\sin(\pi/M)}{\sin^2\eta}\right) d\eta. \tag{14}$$

For binary PSK (BPSK) case, (14) can be easily modified for $M = 2$. Further, under the perfect DF relay assumption, the achievable rate for both transmission scheme is calculated by $R_{\text{Hybrid}} = \log_2(1 + \gamma_{\text{tot}})$.

On the other hand, we analyze the achievable rate performance of our hybrid RIS and relay transmission schemes, and propose the sequential phase and power optimization algorithm in order to maximize the achievable rate under the non-ideal DF relay assumption. The decoding performance of the transmitted symbol degrades as the distance between the S and the relay increases. In this case, the transmit power may be adjusted to ensure that the maximized performance metrics are obtained. Under the non-ideal DF relay, the achievable rate is calculated by

$$R_{\text{Hybrid}}^i = 1/2 \log_2\left(1 + \min\left\{\gamma_r^i, \gamma_{tot}\right\}\right), \; i \in \{1, 2\} \tag{15}$$

where γ_r^1 and γ_r^2 is the received SNR at the relay for joint ($i = 1$) and integrated ($i = 2$) RIS and relay case. In order to obtain a maximized rate for the hybrid RIS and relay configuration in the joint RIS and relay transmission, the corresponding power optimization problem is formulated as

$$\begin{aligned} R_{\text{Hybrid}}^1 = \max_{P_1} \quad & \min\left(\frac{P_1 |\mathbf{g}_{\text{R}}^T \mathbf{\Phi_1} \mathbf{h}_{\text{SR}}|^2}{N_0}, \frac{P_2 \text{A}^2}{N_0} + \frac{P_2 \text{B}^2}{N_0}\right) \\ \text{s.t.} \quad & P_2 = (P_{\text{tot}} - P_1)/2, \quad P_1 < P_{\text{tot}} \end{aligned} \tag{16}$$

Here, we assumed that $P_2 = P_3$ to have a convex optimization problem. Thus, the power constraint in (16) is set by considering $P_t = P_1 + 2P_2$. The corresponding optimization problem for integrated RIS and relay case at D in the second time slot is expressed as

$$\begin{aligned} R_{\text{Hybrid}}^2 = \max_{P_1} \quad & \min\left(\frac{P_1 |g_{\text{SR}}|^2}{N_0}, \frac{P_2 \text{A}^2}{N_0} + \frac{P_2 \left|g_{\text{RD}}\right|^2}{N_0}\right) \\ \text{s.t. } & P_2 = P_{\text{tot}} - P_1, \quad P_1 < P_{\text{tot}} \end{aligned} \tag{17}$$

Since S does not transmit in both time slots for the integrated RIS and relay scheme, the power constraint in (17) is set by considering $P_t = P_1 + P_2$. Here, the total power should be allocated between first and second time slots, in order to enhance system performance. To this end, sequential phase and power optimization algorithm is proposed to sequentially optimize the phase responses of the RIS elements and transmit powers in order to obtain the maximized rate. In this algorithm, the inputs are selected according to corresponding concept. First, $\mathbf{\Phi_1}$ and $\mathbf{\Phi_2}$ are optimized to maximize the received SNR in both time slots. Then, using this phase matrices, end-to-end channel expressions are obtained to modify SNR expressions. In the last step, the optimal value of P_1 is calculated by using the CVX tool [14] to maximize the rate and iteratively search for this optimal value until the objective function converges. Here, the complexity of Algorithm 1 depends on the number of iterations. The overall steps of the sequential algorithm to solve (16) and (17) are summarized in Algorithm 1.

IV. Numerical Results

In this section, we illustrate the error and achievable rate performances of the proposed hybrid schemes via numerical simulations by considering path loss as well as channel fading. Rician factor is assumed as $K = 10$ dB for all simulations, and path loss is modeled using the 3GPP Urban Micro (UMi) [15] and 5G UMi-Street Canyon [16] path loss models for 2.4 GHz and 28 GHz, respectively. Here, we consider a two-dimensional (2D) coordinate system for the positioning of the terminals, which are located in the xy-plane.

Figs. 3(a) and (b) demonstrate the theoretical and simulated average bit error rate (BER) performances of the proposed hybrid schemes with respect to SNR, which is defined as

Authorized licensed use limited to: ULAKBIM UASL - KOC UNIVERSITY. Downloaded on May 09,2021 at 19:32:20 UTC from IEEE Xplore. Restrictions apply.

Algorithm 1 Sequential Phase and Power Optimization

if Joint RIS and relay transmission scheme **then**.
  Input: $N_0, P_t, \mathbf{h}_{\text{SR}}, \mathbf{h}_{\text{RD}}, \mathbf{g}_{\text{R}}, g_{\text{RD}}$.
  Set $P_2 = (P_t - P_1)/2$.
  Optimize $\mathbf{\Phi_1}$ and $\mathbf{\Phi_2}$ by yielding the largest value of (4) and (7), respectively.
  Obtain A, B by using input channels, $\mathbf{\Phi_1}$ and $\mathbf{\Phi_2}$.
  Find optimal solution to P_1 and P_2 via CVX yielding the largest value of (16)
  return $P_1, \mathbf{\Phi_1}, \mathbf{\Phi_2}$.
else (Integrated RIS and relay transmission scheme)
  Input: $N_0, P_t, \mathbf{h}_{\text{SR}}, \mathbf{h}_{\text{RD}}, g_{\text{SR}}, g_{\text{RD}}$.
  Set $P_2 = P_t - P_1$.
  Optimize $\mathbf{\Phi_1}$ by yielding the largest value of (13).
  Obtain A by using input channels and $\mathbf{\Phi_1}$.
  Find optimal solution to P_1 and P_2 via CVX yielding the largest value of (17)
  return $P_1, \mathbf{\Phi_1}$

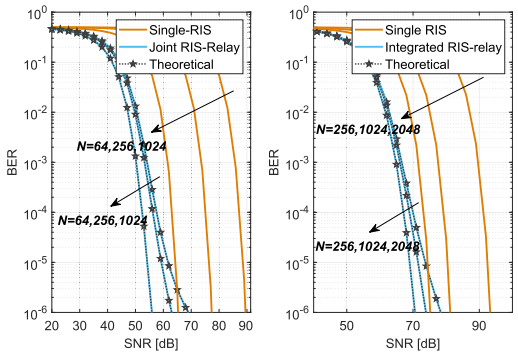

Fig. 3. BER performance of the (a) joint, and (b) integrated RIS and relay transmission schemes for increasing N values.

P_{tot}/N_0, for BPSK signaling and $P_1 = P_2 = 5$ W at 2.4 GHz under increasing N. In this comparison, a single RIS-assisted transmission scheme is considered as a benchmark system. As clearly seen from Figs. 3(a) and (b), the theoretical and simulation results are in perfect agreement for both scenarios. In Fig. 3(a), the simulations are conducted for the joint RIS and relay case when coordinates of the S, D, RIS, and the relay in the xy-plane are given as $(5, 0)$, $(5, 10)$, $(0, 15)$, and $(10, 35)$, respectively. Meanwhile, 2D coordinates of the S, D, and the RIS/relay are respectively given as $(40, 0)$, $(40, 75)$, and $(0, 35)$ for the integrated RIS and relay transmission in Fig. 3(b). For both scenarios, increasing N provides a significant improvement in BER over a single RIS-assisted transmission, and doubling N leads to about 5 dB gain in SNR for joint RIS and relay case, while it brings approximately 3 dB gain for integrated RIS and relay case. Since the effect of the relay in transmission diminishes for large N values, the BER performances of the single-RIS and hybrid schemes get closer to each other. It demonstrates that joint RIS and relay transmission scheme appears to be more efficient than the integrated RIS and relay scheme in terms of BER performance. Furthermore, the overhead of channel estimation will increase due to the link between RIS and relay in the joint RIS and relay transmission scheme while the integrated RIS and relay scheme leads to a similar overhead of channel estimation as the existing RIS-assisted transmission scenarios in the literature.

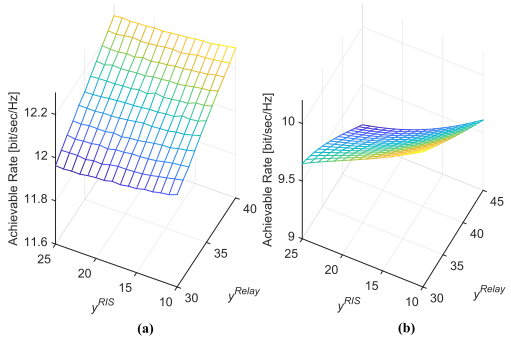

Fig. 4. Achievable rate of the joint RIS and relay scheme when (a) ideal and (b) non-ideal relaying are considered for a varying distance in the y-axis between the RIS and the DF relay.

In Figs. 4(a) and (b), the effect of varying RIS and relay positions in the y-axis on the achievable rate performance of the joint RIS and relay transmission scheme is investigated under perfect and imperfect DF relay assumption for $P_1 = 5$ W, $P_2 = 2.5$ W, $N_0 = -130$ dBm and $N = 2048$ at 28 GHz. Here, the S, D, RIS, and the relay are located at $(10, 0)$, $(10, 60)$, $(0, y^{\text{RIS}})$ and $(25, y^{\text{Relay}})$ in the xy-plane, respectively. As seen from Fig. 4(a), the best achievable rate performance is obtained when the RIS is close to S and the relay is close to D, while the proximity of the ideal relay to D is a more dominant factor in this scheme. On the other hand, as seen in Fig. 4(b), since the RIS plays a more effective role in transmission when the relay does not have perfect decoding capability, the best achievable rate performance is obtained when the RIS is close to the S and the relay close to the RIS. In other words, the existence of a reliable channel between the RIS-relay will play a key role in achievable rate under the non-ideal relay.

In Fig. 5, the achievable rate of the integrated RIS and relay transmission scheme is compared to the single-RIS and single-relay assisted transmission scheme under varying N at 2.4 GHz. Here, the S, D, and the RIS/relay are located at $(20, 0)$, $(20, 55)$, and $(0, 20)$, respectively. As shown, increasing N significantly improves the effect of the RIS in transmission both in the case of the single-RIS and the integrated RIS and relay scheme. Moreover, for the latter scheme, these three cases can be also considered as three different operating modes, and the activation of the RIS and/or relay for transmission can be dynamically determined according to the requirements. In order to increase energy efficiency, if the number of reflecting elements of RIS is enough for a reliable communication, transmission can be conducted over a single RIS, while the hybrid transmission can be conducted by activating the relay to compensate rapid deterioration in the channel quality.

Figs. 6(a) and (b) exhibit the achievable rate comparison of the joint RIS and relay transmission scheme for $P_1 = 5$ W and $P_2 = P_3 = 2.5$ W, and the integrated RIS and relay transmission scheme for $P_1 = P_2 = 5$ W, under changing the RIS position through the y-axis. In order to examine the effect of a finite-level phase adjustment, the case of discrete phase shifts is also considered with two control bits. Here, the S, D, and RIS are respectively located at $(5, 0)$, $(5, 50)$, and $(0, y^{\text{RIS}})$ for both schemes, while the relay is located at

Authorized licensed use limited to: ULAKBIM UASL - KOC UNIVERSITY. Downloaded on May 09,2021 at 19:32:20 UTC from IEEE Xplore. Restrictions apply.

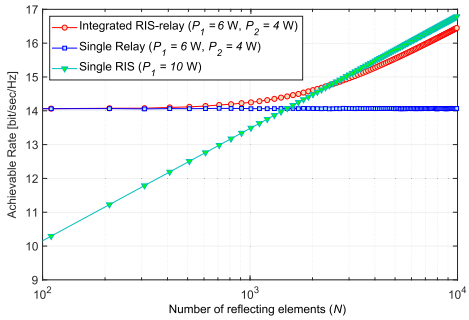

Fig. 5. Achievable rates with the two proposed RIS and DF relay schemes for varying N values.

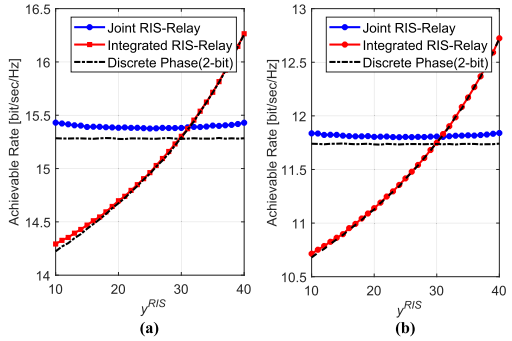

Fig. 6. Achievable rates of the joint and integrated RIS and relay transmission schemes for (a) $N = 256$ at 2.4 GHz and (b) $N = 2048$ at 28 GHz.

$(10, 35)$ for the integrated RIS and relay case. The results shown in Figs. 6(a) and (b) indicate that joint RIS and relay scheme outperforms integrated RIS and relay transmission scheme, although the advantage of the joint RIS and relay case over the integrated RIS and relay case is reduced upon increasing y^{RIS}. More specifically, the best positioning for the RIS is near of the S for the joint RIS and relay transmission, while its proximity to D is the best option for the integrated RIS and relay scheme. Moreover, as clearly seen from Fig. 6, both schemes maintain their advantages in the case of discrete phase adjustment.

In Fig. 7(a), the achievable rate of the joint RIS and relay transmission scheme for varying RIS and relay positions is analyzed by considering the proposed sequential optimization algorithm under the non-ideal relay at 28 GHz. In Fig 7(b), the P_1 values that maximize the rate are plotted for varying RIS and relay locations in the y-axis. Here, $P_{\text{tot}} = 5$ W and the S, D, RIS, and the relay are respectively located at $(10, 0)$, $(10, 40)$, $(0, y^{\text{RIS}})$ and $(0, y^{\text{Relay}})$ in xy-plane. As shown from Fig. 7(a), the achievable rate is maximized when both the RIS and the relay are positioned close to S. If the RIS is positioned far from S, the signal quality at the relay will be deteriorated considerably. Since the perfect decoding assumption is not considered, the signal quality at the relay increases as the relay is located closer to the RIS, therefore, the required P_1 decreases, and more power is assigned to the second-time slot, as seen from Fig. 7(b). In other words, the rate is maximized when the relay is activated and more power assigned to P_2.

V. Conclusion

In this letter, we have proposed two hybrid transmission concepts to improve achievable rate and error performance

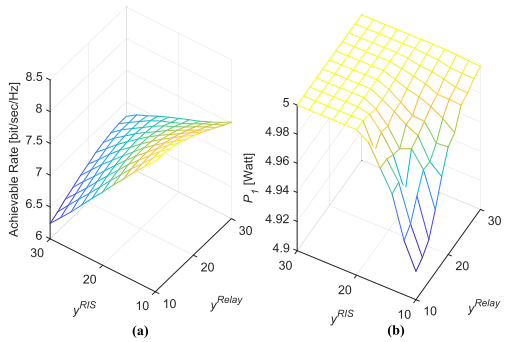

Fig. 7. (a) Achievable rate and (b) P_1 analysis for the joint RIS and relay transmission with the sequential algorithm for $N = 1024$ at 28 GHz.

by exploiting the most important advantages of RIS and relaying technologies. We have shown that these two exciting technologies can work in a harmony with each other under appropriate transmission scenarios. It is also demonstrated through simulations that the relay can be considered as an additional performance-enhancing component to the RIS-assisted transmission scenario especially in the case of rapid deterioration in the channel.

References

[1] E. Basar *et al.*, "Wireless communications through reconfigurable intelligent surfaces," *IEEE Access*, vol. 7, pp. 116753–116773, 2019.
[2] E. Basar and I. Yildirim, "SimRIS channel simulator for reconfigurable intelligent surfaces in future wireless networks," 2020, *arXiv:2008.01448*. [Online]. Available: http://arxiv.org/abs/2008.01448
[3] C. Huang *et al.*, "Holographic MIMO surfaces for 6G wireless networks: Opportunities, challenges, and trends," *IEEE Wireless Commun.*, vol. 27, no. 5, pp. 118–125, Oct. 2020.
[4] E. Basar and I. Yildirim, "Indoor and outdoor physical channel modeling and efficient positioning for reconfigurable intelligent surfaces in mmWave bands," 2020, *arXiv:2006.02240*. [Online]. Available: http://arxiv.org/abs/2006.02240
[5] M. D. Renzo *et al.*, "Smart radio environments empowered by reconfigurable AI meta-surfaces: An idea whose time has come," *EURASIP J. Wireless Commun. Netw.*, vol. 2019, no. 1, pp. 1–20, May 2019.
[6] I. Yildirim *et al.*, "Modeling and analysis of reconfigurable intelligent surfaces for indoor and outdoor applications in future wireless networks," *IEEE Trans. Commun.*, early access, Nov. 3, 2020, doi: 10.1109/TCOMM.2020.3035391.
[7] C. Huang *et al.*, "Reconfigurable intelligent surfaces for energy efficiency in wireless communication," *IEEE Trans. Wireless Commun.*, vol. 18, no. 8, pp. 4157–4170, Aug. 2019.
[8] E. Bjornson *et al.*, "Intelligent reflecting surface versus decode-and-forward: How large surfaces are needed to beat relaying?" *IEEE Wireless Commun. Lett.*, vol. 9, no. 2, pp. 244–248, Feb. 2020.
[9] X. Ying *et al.*, "Relay aided intelligent reconfigurable surfaces: Achieving the potential without so many antennas," 2020, *arXiv:2006.06644*. [Online]. Available: http://arxiv.org/abs/2006.06644
[10] Z. Abdullah *et al.*, "A hybrid relay and intelligent reflecting surface network and its ergodic performance analysis," *IEEE Wireless Commun. Lett.*, vol. 9, no. 10, pp. 1653–1657, Oct. 2020.
[11] Z. Abdullah *et al.*, "Optimization of intelligent reflecting surface assisted full-duplex relay networks," *IEEE Wireless Commun. Lett.*, early access, Oct. 15, 2020, doi: 10.1109/LWC.2020.3031343.
[12] P. Billingsley, *Probability and Measure*, 2nd ed. New York, NY, USA: Wiley, 1995.
[13] M. Simon and M. S. Alouini, *Digital Communications over Fading Channels*, 2nd ed. Hoboken, NJ, USA: Wiley, 2005.
[14] M. Grant *et al.*, (2009). *CVX: MATLAB Software for Disciplined Convex Programming*. [Online]. Available: http://cvxr.com/cvx
[15] *Evolved Universal Terrestrial Radio Access (E-UTRA); Further Advancements for E-UTRA Physical Layer Aspects*, document 3GPP-TR-36.814, 2010.
[16] S. Sun *et al.*, "Propagation path loss models for 5G urban micro-and macro-cellular scenarios," in *Proc. IEEE 83rd Veh. Technol. Conf. (VTC Spring)*, May 2016, pp. 1–6.

Authorized licensed use limited to: ULAKBIM UASL - KOC UNIVERSITY. Downloaded on May 09,2021 at 19:32:20 UTC from IEEE Xplore. Restrictions apply.